Comprehensive Explanation of the Anomalous EPR Spectra of Wild-Type and Mutant Cytochrome *c* Peroxidase Compound ES†

Andrew L. P. Houseman,‡ Peter E. Doan,‡ David B. Goodin,*,§ and Brian M. Hoffman*,‡

Department of Chemistry, Northwestern University, Evanston, Illinois 60208, and Department of Molecular Biology, MB8, The Scripps Research Institute, 10666 North Torrey Pines Road, La Jolla, California 92037

Received October 14, 1992; Revised Manuscript Received February 1, 1993

ABSTRACT: Although the cytochrome *c* peroxidase/H_2O_2 reaction product, compound ES, has been a long-standing subject of research, only recently has its broad EPR signal been proven to arise from a radical at Trp-191. Despite this advance, no model has satisfactorily explained the anomalous breadth and shape of this signal, which is conventionally interpreted as having axial symmetry with $g_\parallel \approx 2.04 > g_\perp \approx 2.01$, contrary to expectations for a planar π radical. Furthermore, these *g* values exhibit marked temperature and preparation dependencies as well as an unexplained high-field "tail" extending from the $g = 2.01$ peak. We have reexamined the EPR and ENDOR spectra of compound ES at 35 GHz, as well as those of compound ES in the mutant D235E. This mutation significantly alters the line shape of the Trp-191 free radical. We present a comprehensive model that successfully accounts for the properties of this unusual protein free radical. We show that the EPR spectra of both proteins can be described in terms of a weak exchange interaction between the $S = 1$ oxyferryl $(Fe{=}O)^{2+}$ moiety and a radical on Trp-191; a distribution in protein conformation leads to a distribution in the coupling, which ranges from ferromagnetic to antiferromagnetic. We also derive, for the first time, explicit expressions for frozen-solution and single-crystal spectra of such spin-coupled systems and show that the model accounts for all the data that previously led to apparent anomalies in the interpretation of the frozen-solution and single-crystal [Hori, H., & Yonetani, T. (1985) *J. Biol. Chem. 260*, 349–355] EPR properties. Finally, we have used the CW EPR and pulsed-EPR saturation–recovery methodology to address reports that the broad signal from the spin-coupled Trp-191 radical is accompanied by a minority (~10%), narrow signal that is associated with a radical site other than Trp-191. We find no evidence for such a species and discuss the earlier reports in light of our model.

Cytochrome *c* peroxidase (C*c*P),[1] first isolated by Altschul from baker's yeast in 1940 (Altschul et al., 1940), catalyzes the H_2O_2-dependent oxidation of ferrocytochrome *c* (Yonetani, 1965; Coulson et al., 1971).

$$C\textit{c}P + H_2O_2 \rightarrow ES + H_2O$$

$$ES + 2\text{Cyt } \textit{c}(\text{Fe II}) + 2H^+ \rightarrow C\textit{c}P + 2\text{Cyt } \textit{c}(\text{Fe III}) + H_2O$$

Like other peroxidases such as horseradish peroxidase (HRP) and catalase, the resting state of C*c*P contains a ferric heme, and the enzyme is capable of storing two oxidizing equivalents following treatment with peroxide (Yonetani, 1965, 1976; Yonetani et al., 1966; Coulson et al., 1971; Dawson, 1988). This fully oxidized reaction intermediate is called compound ES in the case of C*c*P and compound I in the case of HRP and catalase (Lang et al., 1976; Dawson, 1988). One of the equivalents in both compound ES and compound I is stored as the $S = 1$ oxyferryl (Fe(IV)) moiety (Schulz et al., 1979; Roberts et al., 1981; Dawson, 1988). The other equivalent is stored as an organic radical. For compound I this is the π-cation radical of the porphyrin macrocycle, but for compound ES the second equivalent resides on an amino acid residue (Wittenberg et al., 1968; Oosterhuis & Lang, 1973; Hoffman et al., 1979).

The identity of the compound ES radical has been a subject of numerous investigations for a quarter of a century, culminating in the ENDOR experiments on isotopically labeled protein that positively identified the radical with a Trp residue (Sivaraja et al., 1989). This information, combined with data from mutagenesis experiments (Goodin et al., 1986, 1987; Edwards et al., 1987; Fishel et al., 1987; Mauro et al., 1988) and the known crystal structure of compound ES (Finzel et al., 1984), strongly implied that Trp-191 was the radical site (Sivaraja et al., 1989) (Figure 1).

Despite this positive identification, the EPR signal of the compound ES radical is not yet understood. (i) It *appears* to be described by an axial **g** tensor with $g_\perp = 2.01$ and $g_\parallel = 2.04$ at 2 K, but *g* values of such magnitude are unknown and unlikely for an isolated aromatic radical: for a radical, the maximum shift for any component of the **g** tensor from the free-electron *g* value, $g_e = 2.0023$, is invariably $\Delta g_i = |g_i - g_e| \leq 0.01$ (Atherton, 1973; Box, 1977; Gordy, 1980). Indeed, the EPR spectrum of the Trp cation radical has a breadth of only 21 G in frozen solution at X band (Moan & Kaalhus, 1974), equivalent to $\Delta g = 0.013$. (ii) The **g** tensor of an isolated, planar π radical is axial but has $g_\perp > g_\parallel$ (Atherton,

† This work was supported in part by NIH Grants GM41049 to D.B.G. and HL13531 to B.M.H. and by NRSA Training Grant T32 GN08382.

* Author to whom correspondence should be addressed.
‡ Northwestern University.
§ The Scripps Research Institute.

[1] Abbreviations: C*c*P, cytochrome *c* peroxidase; ENDOR, electron nuclear double resonance; EPR, electron paramagnetic resonance; ES, reaction product of C*c*P with H_2O_2; HRP, horseradish peroxidase.

0006-2960/93/0432-4430$04.00/0

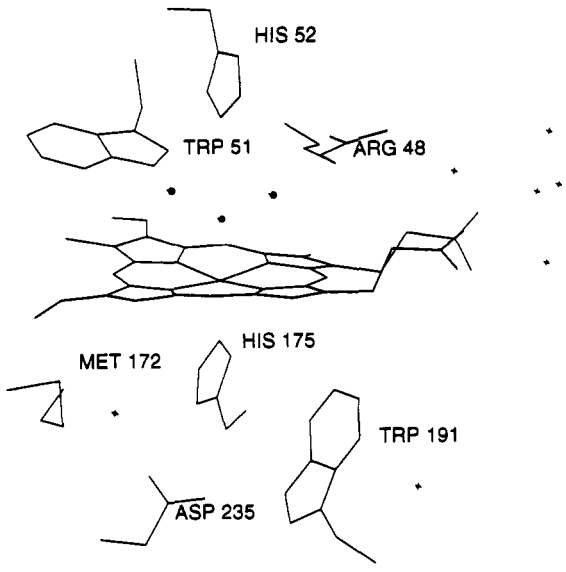

FIGURE 1: Active site of cytochrome c peroxidase (Finzel, 1984) showing Trp-191, the radical site of compound ES, nearly perpendicular to the heme plane. Asp-235 forms a hydrogen bond with Trp-191 and with His-175, the proximal heme ligand. The figure was prepared with the program XFIT (McRee, 1992).

1973) in contrast to the case for compound ES. (iii) The compound ES EPR signal is strongly temperature-dependent (Wittenberg et al., 1968) and contrary to the case of the organic radicals but like that of horseradish peroxidase (HRP) (Hoffman et al., 1979; Schulz et al., 1979). (iv) There is great variability in the apparent g values, in part because the edges of the EPR spectra of compound ES are poorly resolved (Wittenberg et al., 1968; Hoffman et al., 1981; Hori & Yonetani, 1985). Indeed, several researchers have commented that the apparent $g_{\|}$ and $g_{\perp}$ values vary with sample preparation (Wittenberg et al., 1968; Hoffman et al., 1979; Hori & Yonetani, 1985). (v) Finally, the EPR envelope of compound ES has a large high-field "tail" (toward $g < 2$) that no model to date has satisfactorily explained (Hoffman et al., 1979).

The $S = {}^1/_2$ Trp radical of compound ES is associated with a paramagnetic, $S = 1$, oxyferryl heme, and an obvious and attractive explanation for these anomalies would be that they result from spin coupling between the two centers. A well-defined exchange interaction could lead to an axial g tensor with g shifts of $|\Delta g| \leq 0.05$ (Hoffman et al., 1979). However, the theory predicts $g_{\perp} > g_{\|} \approx 2.00$ in contrast to the conventional interpretation of the EPR spectrum of compound ES, with $g_{\|} > g_{\perp} \approx 2.00$.

In this paper we present a comprehensive model which successfully accounts for the observed properties of this unusual protein free radical. In the process of developing and testing this model, we have reexamined the EPR and ENDOR spectra of compound ES at 35 GHz, as well as those of the Asp-235 → Glu mutant, ES(D235E). ^{1}H ENDOR measurements are reported on compound ES with natural isotopic abundance (ES(H,H)), on compound ES prepared with Trp-d_8 and exchanged into D_2O (ES(d_8,D)), and ES(D235E). The D235E mutation, which perturbs the protein structure only slightly (Goodin & McRee, 1992), significantly alters the line shape of the Trp-191 free radical. We show that each of these spectra can be described in terms of a weak exchange interaction between the $(Fe{=}O)^{2+}$ and a radical on Trp-191; a distribution in protein conformation leads to a distribution in the coupling, which ranges from ferromagnetic to antiferromagnetic. Such a model was first introduced to explain the EPR spectrum of HRP, which shows coupling between the $(Fe{=}O)^{2+}$ and a radical on the protoporphyrin ring itself (Schulz et al., 1979). We have also derived, for the first time, explicit expressions for frozen-solution and single-crystal spectra of such spin-coupled systems and show that the model accounts for all the data that previously led to apparent anomalies in the interpretation of the frozen-solution (Yonetani et al., 1966; Hoffman et al., 1979, 1981) and single-crystal (Hori & Yonetani, 1985) EPR properties.

Finally, we have used the pulsed-EPR saturation–recovery methodology (Hyde, 1979) to address reports that the broad signal from the spin-coupled Trp-191 radical is accompanied by a minority (~10%), narrow signal that is associated with a radical site other than Trp-191, one remote from the heme (Hori & Yonetani, 1985). We find no evidence for such a species and discuss the earlier reports in light of our model. The present results also are used to discuss EPR spectra in a variety of mutants that exhibit such narrow signals (Scholes et al., 1989; Fishel et al., 1991).

MATERIALS AND METHODS

Sample Preparation. The wild-type CcP used in this study was CcP(MKT), which contains Met-Lys-Thr on the N-terminus. It was produced in *Escherichia coli* from the plasmid pT7CcP under control of the T7 promoter (Goodin et al., 1991; Goodin & McRee, 1992). Purified protein made by this method exhibits normal functional properties and gives optical and EPR spectra in the native and compound ES states that are unaltered from those of the protein isolated from yeast. The preparation of the mutant D235E is described elsewhere (Goodin & McRee, 1992). Procedures for producing CcP containing deuterated tryptophan are described by Sivaraja et al. (1989).

Samples of compound ES were prepared from the enzyme in the ferric state (about 1 mM) in 100 mM potassium phosphate, pH 6, buffer containing 30% glycerol (v/v) by the addition of H_2O_2 in a 5-fold stoichiometric excess. They were frozen rapidly and stored at 77 K. The sample of compound ES from the mutant D235E was prepared by adding a 2-fold excess of H_2O_2 to the protein in 60% glycerol (v/v).

EPR Spectroscopy. EPR spectra were taken at 2 K with a modified Varian Associates 35-GHz spectrometer, using 100-kHz field modulation and dispersion-detection mode under conditions of adiabatic rapid passage. These conditions yield spectra that correspond to the undifferentiated EPR absorption envelope. As needed, the spectra were differentiated numerically. EPR simulations employed the program QPOW (University of Illinois). EPR simulations using the distribution model were performed with the program MathCad on an IBM-compatible PC.

Saturation–recovery experiments were performed with an X-band pulsed EPR spectrometer that is described elsewhere (Fan et al., 1992). A portion of the EPR spectrum was saturated using a series of four $\pi/2$ pulses of ca. 64 ns applied over a period of 1.1 μs. The times between these pulses were of unequal lengths, varying between 200 and 500 ns. The height of a subsequent two-pulse ($\pi/2 - \pi$) echo was recorded as a function of the evolution time, T, between the last pulse of the saturating sequence and the start of the detection sequence. The occurrence of complete saturation was confirmed by the absence of a two-pulse echo for $T \rightarrow 0$.

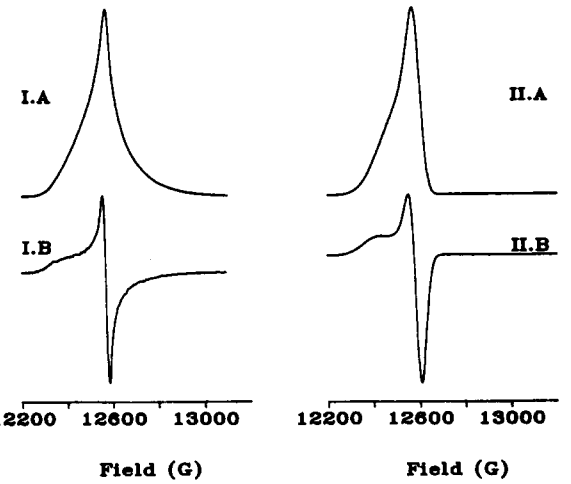

FIGURE 2: I. K_a Band EPR spectrum at 2 K. (A) Absorption spectrum; (B) first derivative of spectrum in panel A. II. QPOW simulation of EPR spectrum using g = [2.04, 2.01, 2.01] and W = [200, 70, 70] MHz. (A) Absorption; (B) first derivative.

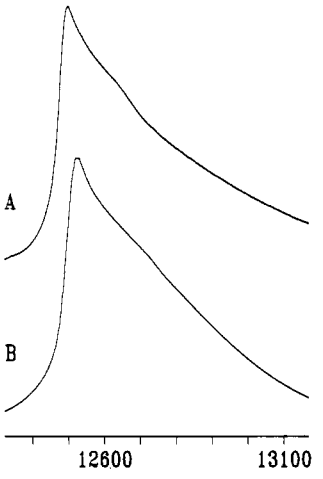

FIGURE 3: EPR spectra of D235E mutant. (A) Absorption spectrum. Conditions: 0.05 mW of microwave power, 35.005 GHz, 8 G modulation amplitude. (B) Simulation using a distribution model with $g_\parallel$ = 2.00, $B_\parallel$ = 12 510 G; $\bar{\delta}$ = –0.04, σ = 0.04; W = 15 G.

RESULTS AND ANALYSIS

EPR and ENDOR of Wild-Type Compound ES and ES(D235E)

EPR. Figure 2I.A shows the EPR absorption envelope of compound ES in frozen solution, taken at 35 GHz and 2 K. Comparison with spectra taken at ~9 GHz shows that the shape of the spectrum is independent of the microwave frequency, confirming that this shape is determined by the Zeeman interaction (Hoffman et al., 1981). The absorption envelope has its maximum at g = 2.01 and a shoulder to lower field at g = 2.04 (Figure 2I.A). The derivative of this spectrum is dominated by these features and appears at first glance to have axial symmetry with $g_\parallel$ = 2.04 and $g_\perp$ = 2.01 (Figure 2I.B). However, it is apparent that the absorption envelope also has a long, featureless tail to high field that is obscured in the more standard derivative presentation.

Hoffman et al. (1979) found that the low- and high-field portions of the derivative spectrum could not be adequately simulated simultaneously. For comparison we show in Figure 2II.B the best low-field simulation that could be obtained using parameters for a single species with g = [2.04, 2.01, 2.01] and a highly anisotropic line width ($W_\parallel$ = 70 and $W_\perp$ = 200 MHz). This simulation can reproduce the low-field part of the experimental spectrum, but it is wholly inadequate to simulate the high-field portion. Thus, neither absorption nor derivative presentation can be adequately described in terms of a conventional axial **g** tensor. The introduction of this paper enumerated additional reasons why the apparent g components could not be associated with an isolated π radical.

Site-specific mutagenesis provides a means of probing the origin and nature of the compound ES EPR spectrum. Fishel et al. (1991) have presented EPR spectra for compound ES from a number of mutated proteins. In general, a single-site mutation either gave a protein with a spectrum generally similar to the "broad" spectra in Figure 2 or else abolished the broad spectrum and only a narrow free radical signal was seen. In contrast, the Asp-235 → Glu mutant gives a broad signal (Figure 3) that is startlingly different from that of the native protein. Nearly all the intensity that has been viewed as *the* characteristic of the broad signal, that with g > 2.0, has disappeared. Instead, the absorption envelope has a maximum at g = 1.985 and trails to higher field (lower g). The spectrum again *appears* to have axial symmetry, but with $g_\perp$ = 1.997 > $g_\parallel$ = 1.975. The X-ray structure of wild-type C*c*P suggests that residue 235 would be central to the exchange coupling because the carboxyl group of Asp-235 forms a hydrogen-bond bridge between the proximal histidine ligand and Trp-191. The X-ray structure of D235E shows that the bridge persists, although slightly perturbed; this minor perturbation dramatically changes the EPR spectrum of compound ES (Goodin & McRee, 1992).

ENDOR. To determine whether the entire EPR envelope of compound ES in Figure 3 belongs to the same radical site, we collected ENDOR spectra on compound ES in H_2O (ES(H,H)) at multiple fields across the EPR envelope (2.05 ≤ g ≤ 1.984) and compared them to spectra taken from a D_2O solution of compound ES prepared from protein grown on tryptophan-d_8 (ES(d_8,D)). ENDOR spectra also were collected from perprotonated ES(D235E) in H_2O buffer to test whether its anomalous EPR spectrum is associated with the same radical site as in the wild-type enzyme.

The top spectrum of Figure 4A shows ^{1}H ENDOR of ES(H,H) at the low-field edge of the EPR envelope of wild-type protein, g = 2.040. As reported earlier, the spectrum of compound ES shows numerous doublets centered at ν_H with splittings in the range 2 ≲ A^H ≲ 22 MHz (Sivaraja et al., 1989). The top spectrum of Figure 4B is ENDOR of ES(D235E) mutant taken at the same g value. The EPR spectrum of this mutant does not have significant intensity at fields below g ≈ 2.0, and thus, as expected, an ENDOR spectrum taken at this field is extremely weak, with the most significant feature being a matrix peak associated with an underlying EPR signal from unoxidized low-spin Fe^{3+}C*c*P (Figure 4B, top).

The middle spectra of Figure 4A,B are ^{1}H ENDOR from ES(H,H) and ES(D235E), respectively, and are taken at the position of greatest EPR intensity for both native and mutant protein, g ≈ 2.0. The inset spectrum of Figure 4A, middle, is ^{1}H ENDOR of ES(d_8,D). As reported earlier, perdeuteration of Trp eliminates all local ^{1}H hyperfine coupling, and the only signal seen is a sharp protein-matrix ENDOR peak at the proton Larmor frequency. This is the result that shows the radical to be located on a Trp. ES(H,H) gives the expected

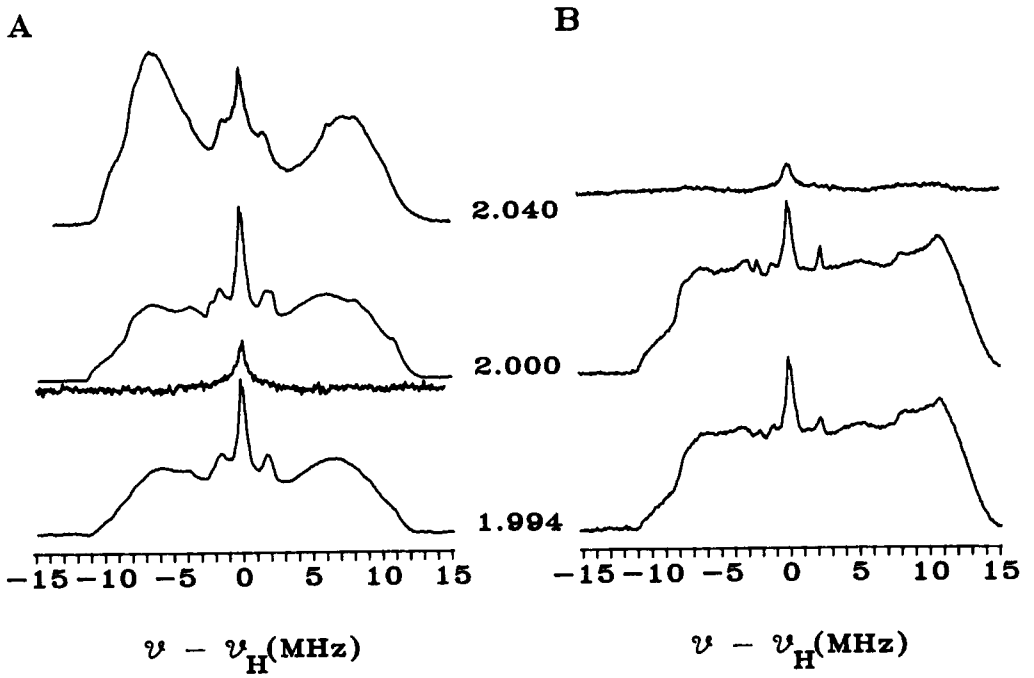

FIGURE 4: ^{1}H ENDOR spectra of ES(H,H) (A) and ES(D235E) (B). A spectrum of ES(d^8,D) at $g = 2.00$ is included below that of ES(H,H). Conditions: microwave frequency, (A) 35.29 GHz, (B) 35.005 GHz; ES(d^8,D), 35.485 GHz; microwave power, 0.05 mW; 8 G modulation amplitude; modulation frequency, 100 kHz; rf power, 20 W; rf sweep rate, 1 MHz/s; time constant, 0.032 s; magnetic field, (A) top 12 360 G, middle 12 607 G, bottom 122 709 G, B) top 12 260 G, middle 12 505 G, bottom 12 606 G; ES(d^8,D), 12 677 G.

^{1}H pattern for the perprotonated Trp-191 radical, and ES(D235E) gives a nearly identical spectrum. This shows that the radical site is, in fact, the same in both the mutant and wild-type proteins. The only significant difference between the native and mutant spectra is on the ν_+ side. Although the frequency of each feature is identical, the intensities differ, particularly at $\delta\nu \equiv (\nu - \nu_H) \approx +11$ MHz ($A \approx 22$ MHz). This merely reflects a change in spin relaxation, but not in hyperfine coupling. Finally, the bottom spectra of Figure 4A,B are also from ES(H,H) and ES(D235E) and were taken at $g = 1.984$. The spectrum of the mutant (Figure 4B, bottom) again matches that of the native protein (Figure 4A, bottom). Indeed, spectra of ES(H,H) and ES(D235E) taken at numerous fields for $g \leq 2.00$ (data not shown) are virtually the same at every field.

In both wild-type and mutant proteins, details of the spectra change with field. However, close observation reveals that features do not change position in frequency, but rather they change in line width and/or intensity. The ^{1}H hyperfine couplings of compound ES, therefore, *appear* isotropic in agreement with earlier experiments, and the same is true for the mutant. These measurements make it clear that the EPR envelopes of both wild-type and D235E mutant compound ES differ sharply in appearance, but in both cases they are associated with the Trp-191 radical.

Does the EPR Signal Reflect Well-Defined Heme–Radical Spin Coupling? The unusual features of the EPR signal associated with Trp-191 in compound ES indicate that the signal cannot be associated with an isolated radical, as deduced from LEFE measurements by Lerch et al. (1981). We first consider whether the apparently anomalous features might be the consequences of a *well-defined* heme–radical coupling. We show that such an interaction also cannot explain the behavior of compound ES and then proceed to show that the presence of a distribution in the exchange coupling can do so.

The spin-coupled system of an $S^{Fe} = 1$ Fe(IV)=O and $S^R = {}^1/_2$Trp can be described by the following spin Hamiltonian:[2]

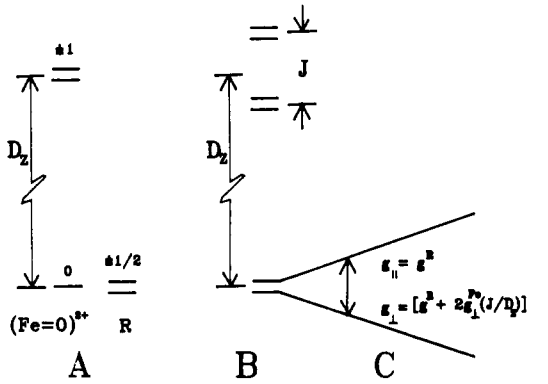

FIGURE 5: Energy level diagram showing (A) isolated $S^{Fe} = 1$ and $S^R = {}^1/_2$ spin states, (B) mixed "$^3/_2$" spin states, and (C) mixed spin states in the presence of a magnetic field. In panel C only the lower levels are shown because at $T \leq 4.2$ K only these are populated and give an EPR transition.

$$\mathcal{H} = S^{Fe}\cdot\mathbf{D}\cdot S^{Fe} - JS^{Fe}\cdot S^R + \beta(S^{Fe}\cdot\mathbf{g}^{Fe}\cdot B + S^R\cdot\mathbf{g}^R\cdot B) \quad (1)$$

The $S^{Fe} = 1$ state of the oxyferryl heme in both HRP and compound ES exhibits axial zero-field splitting, represented by the first term in eq 1. The unique axis lies along the Fe=O bond and has a tensor component, $D_z \approx 22$ cm^{-1} (Schulz et al., 1979), that removes the spin degeneracy and places the $m_s^{Fe} = \pm 1$ spin states at energy D_z relative to the $m_s^{Fe} = 0$ ground state (Figure 5A). An exchange interaction, represented by the second term in eq 1, couples the $S^{Fe} = 1$ spin state of the heme with the $S^R = {}^1/_2$ spin state of the radical, producing the six zeroth-order microstates, $|m_s^{Fe}, m_s^R\rangle = |\pm 1, \pm {}^1/_2\rangle$ and $|0, \pm {}^1/_2\rangle$. For small $|J/D|$ ($< {}^2/_9$), as is the case here, the $|0, \pm {}^1/_2\rangle$ Kramers doublet is the ground state with

[2] The treatment of spin coupling in HRPI by Schulz et al. actually was couched in terms of a J tensor, $-S^{Fe}\cdot\mathbf{J}\cdot S^R$ (and thus a δ tensor). In the case of isotropic coupling this leads to the exchange term in eq 1. We recognize that the two prevalent conventions write such a term as $-2JS^{Fe}\cdot S^R$ or as $+JS^{Fe}\cdot S^R$. However, to provide a direct comparison to the work of Schulz et al., we have followed their example.

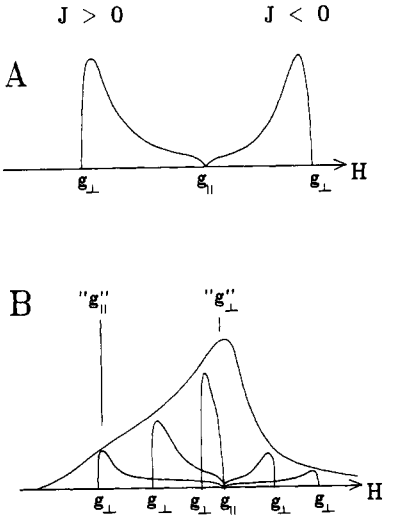

FIGURE 6: Qualitative descriptions of EPR spectra from spin-coupled systems. (A) Ferromagnetically coupled spectrum (lower field) and antiferromagnetically coupled spectrum (higher field). (B) Distribution model of spin-coupled system in which many component EPR spectra like those in panel A add to create an envelope that is qualitatively different in shape from those of the component spectra.

g values that are determined by the magnitude and the sign of the exchange integral, J (Figure 5B). As first described by Schulz et al., to first order

$$g_{\parallel}^{ES} \approx g^{R} = 2.0$$

$$g_{\perp}^{ES} \approx g_{\parallel}^{ES} + 2g_{\perp}^{Fe}(J/D)$$

$$\approx 2.0 + \delta \qquad \delta \equiv 2g_{\perp}^{Fe}(J/D) \tag{2}$$

where $g_{\parallel}^{ES}$ for the spin-coupled system lies parallel to the heme normal (Fe=O bond vector), $g^{R} \approx 2.0$ is the g value of the isolated radical, and $g_{\perp}^{Fe} \approx 2.25$ is the $g_{\perp}$ value for the isolated oxyferryl heme (Schulz et al., 1979; Hoffman et al., 1981). An antiferromagnetic (or bonding) interaction between the radical and the heme is represented by $J < 0$, while $J > 0$ implies ferromagnetic coupling. In principle, J can take either positive or negative values. Thus, $g_{\perp}^{ES}$ can be greater than or less than 2.0, whereas the exchange does not shift $g_{\parallel}^{ES}$ to first order. As an illustration, Figure 6A shows how EPR spectra would appear with $\delta > 0$ (spectrum to low field) and $\delta < 0$ (spectrum to high field). Both have $g_{\parallel}$ at 2.0. This calculation is in *qualitative* disagreement with the conventional interpretation of the derivative EPR spectrum of compound ES, which appears to have an axial **g** tensor with $g_{\parallel} > g_{\perp} \approx 2.0$.

Distributed Spin Coupling and Frozen-Solution EPR of Compound ES

The clue to understanding the EPR spectrum of compound ES lies in the fact that the EPR absorption envelope of compound ES does not have the shape conferred by an axial **g** tensor but shows considerable symmetry about $g \approx 2.01$ (Figure 2I.A). As described above, the high-field tail is suppressed in the derivative spectrum (Figure 2I.B), and it has not been noted except in reference (Hoffman et al., 1979).

The absorption envelope for frozen-solution compound ES in fact is quite reminiscent of that for HRP, which Schulz et al. (1979) described in terms of a spin-coupled system with a distribution in the exchange integral, J (eq 1), and therefore in the g-shift parameter, δ (eq 2) [see also Guigliarelli et al. (1986)]. A simple distribution of J about some most probable value (a normal distribution, for example) then would correspond to a distribution in conformations about some most probable conformation. An EPR spectrum that requires a more complex distribution in $\delta(J)$ could be interpreted in terms of a superposition of several simple distributions and would correspond to several dominant sets of conformations.[3]

In this section and below we show that the presence of a distribution in the spin coupling explains not only the spectra seen in frozen solution but also those observed in single crystals of compound ES. The essence of this model is illustrated in Figure 6B, which is a cartoon representation of the overall EPR envelope that might be expected from a frozen-solution sample that contains molecules with $\delta > 0$ and $\delta < 0$, with the probability density for the occurrence of a given δ decreasing as $|\delta|$ increases. At any given field, EPR spectra (such as those in Figure 6A) from molecules with different values of δ contribute to the intensity. The total intensity at a field is the sum of these contributions. Thus, despite the fact that each component has its maximum at some $|\Delta g| = |g(\delta) - g_{\parallel}| > 0$, it should not be surprising that the result might be a peak near $g_{\parallel}$ that gives a "$g_{\perp}$" feature in a derivative display. Likewise, if the distribution is not centered at $\delta = 0$, one might observe an apparent "$g_{\parallel}$" feature in the derivative. The following analysis confirms this intuition.

Analysis of Frozen-Solution EPR. The observed g value for a particular molecule in a frozen solution is determined by θ, the polar angle that the magnetic field vector makes with the unique, $g_{\parallel}$ axis, as well as the g-shift parameter, $\delta \propto J$, for that molecule. The g value depends on δ and θ through the equation

$$g^2(\delta,\theta) = g_{\parallel}^{\,2}\cos^2(\theta) + g_{\perp}^{\,2}(\delta)\sin^2(\theta)$$

$$= g_{\parallel}^{\,2}\cos^2(\theta) + (g_{\parallel} + \delta)^2\sin^2(\theta) \tag{3}$$

$$\approx g_{\parallel}^{\,2} + 2g_{\parallel}\delta\sin^2(\theta) \tag{4}$$

where we may neglect the term in δ^2 because $\delta/g_{\parallel} \ll 1$. The resonant field, $B(\delta,\theta)$, depends on δ and θ through the g value:

$$B(\delta,\theta) \equiv h\nu/g(\delta,\theta)\beta \tag{5}$$

In a frozen solution, θ is an independent random variable. The probability that $g_{\parallel}$, which lies along the Fe=O bond of a molecule, has an orientation in the range θ to $(\theta + d\theta)$ is

$$p_1(\theta)\,d\theta = \sin(\theta)\,d\theta \qquad \text{for } 0 \le \theta \le \pi/2 \tag{6}$$

In the model to be explored, the g-shift parameter, δ (eq 2), for an ensemble of molecules also is a random variable. The probability that a subset of molecules has a g-shift parameter in the range δ to $(\delta + d\delta)$ is denoted $p_2(\delta)\,d\delta$. The theoretical development does not depend on the form of the probability density, $p_2(\delta)$. In our application of this model, however, we choose to describe $p_2(\delta)$ as a weighted sum of normal (Gaussian) probability density functions, where each is centered around a most probable value, $\bar{\delta}_i$, with variance, σ_i^2,

[3] Schulz et al. characterized HRPI with distributions around the three principal values of a spin-coupling tensor, $\mathbf{J} = [-1.4, 0.7, 0.7]$ cm^{-1}. However, the EPR spectra can be equally well reproduced by a Heisenberg Hamiltonian with J described by a sum of three simple distributions.

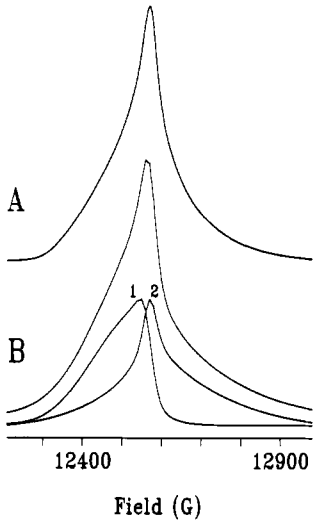

FIGURE 7: Comparison of experimental and simulated frozen-solution EPR spectra. (A) Spectrum of ^{13}C-labeled compound ES at 2 K. Conditions: 0.05 mW microwave power, 35.29 GHz, 8 G modulation amplitude. (B) Simulation using a sum of two-component spectra with equal weights. The first component spectrum labeled 1 has $\bar{\delta} = 0.02$, $\sigma = 0.02$, $g_\parallel = 2.01$, and $B_\parallel = 12\,580$ G. The second component spectrum labeled 2 has $\bar{\delta} = -0.01$, $\sigma = 0.04$, $g_\parallel = 2.01$, and $B_\parallel = 12\,580$ G. EPR line width, W = 18 G.

and each contributes with a fraction, f_i, where $\sum_i f_i = 1$:

$$p_2(\delta) = \sum_{i=1}^{n} \frac{f_i}{\sigma_i\sqrt{2\pi}} \exp\left[\frac{-1}{2}\left(\frac{\delta - \bar{\delta}_i}{\sigma_i}\right)^2\right] \quad (7)$$

In the limit that the component line width for an individual molecule is negligible, then the intensity of the powder-pattern envelope represents the sum of signals at field B from all molecules for which the independent, random variables (θ,δ) give the g value that corresponds to that field (eqs 4 and 5); this intensity is denoted $I_p'(B)$. As described in Appendix A, $I_p'(B)$ is obtained by properly weighting and adding these joint probabilities at field B (Raghunathan, 1987), and the calculation gives the formula

$$I_p'(B) = \sum_{i=1}^{n} \frac{f_i}{\sigma_i\sqrt{2\pi}} \int_0^{\pi/2} \frac{B_\parallel^2}{B^3} \frac{g_\parallel^2}{\sin\theta} \exp\left[-\frac{1}{2}\left(\frac{\delta(\theta,B) - \bar{\delta}_i}{\sigma_i}\right)^2\right] d\theta \quad \text{(A10)}$$

The envelope function actually observed in an EPR spectrum, $I_p(B)$, differs from $I_p'(B)$ by the fact that the spectrum of an individual molecule has a nonzero component width. It is obtained as a convolution of $I_p'(B)$ over the component line shape function, $S(B - B')$,

$$I_p(B) = \int_0^\infty I_p'(B) S(B' - B)\, dB' \quad (8a)$$

$$= \frac{1}{W\sqrt{2\pi}} \int_0^\infty I_p(B') \exp\left[-\frac{1}{2}\left(\frac{B - B'}{W}\right)^2\right] dB' \quad (8b)$$

where eq 8b embodies the explicit assumption that the component line shape is a Gaussian, with W as the intrinsic EPR line width.

Interpretation of Frozen-Solution EPR Spectra of Compound ES and ES(D235E). Figure 7 shows that the full EPR envelope of wild-type compound ES is extremely well reproduced by the distribution model as embodied in eq 8 when $p_2(\delta)$ (eq 7) is chosen to be a sum of two simple density functions ($n = 2$). Figure 7B shows the full simulation using eq 8b along with the individual contributions from the two-component density functions. Component 1 generates the EPR intensity for $g > g_\parallel$ and is responsible for the broad signal generally associated with compound ES; in particular, it produces the low-field shoulder at $g \approx 2.04$ seen both in the simulation and in experimental EPR spectra. This component has $\bar{\delta}_1 = 0.02$ as its most probable value and a width of $\sigma_1 = 0.02$, and it actually represents a minority form with $f_1 = 0.33$. The second (majority) component density function ($f_2 = 0.67$) is centered at $\bar{\delta}_2 = -0.01$ and is much broader ($\sigma_2 = 0.04$). This component generates the tail to high field in the experimental spectrum (Figure 7A). The simulations employed the Gaussian component line shape of eq 8b, with an intrinsic EPR line width, $W = 15$ G, or $W \approx 40$ MHz at $g \approx 2$. This width is consistent with the breadth of the hyperfine pattern that is predicted from the ^{1}H ENDOR measurements presented above. The presence of a number of protons exhibiting coupling of $15 \lesssim A^H \lesssim 20$ MHz would produce an EPR pattern with a width of ~30–60 MHz.

If one takes $D_z \approx 22$ cm^{-1} (Schulz et al., 1979), then according to eq 2 the value $\bar{\delta}_1 = +0.02$ corresponds to a most probable exchange coupling, $\bar{J}_1 \approx +0.098$ cm^{-1}. The positive sign indicates that the molecules associated with component 1 experience predominantly ferromagnetic coupling. Similarly, the most probable exchange coupling for the second component, with $\bar{\delta}_2 = -0.01$ is $\bar{J}_2 \approx -0.049$ cm^{-1}, and is antiferromagnetic.

The model provides an equally satisfactory explanation for and simulation of the EPR response for the compound ES state of the Asp-235 → Glu mutant. Comparison of its EPR spectrum in Figure 3 with the simulation for the wild-type protein (Figure 3C) shows that the change in the mutant spectrum primarily reflects a loss of component 1 of the wild-type distribution. Indeed, the spectrum for the mutant can be simulated with a single distribution with $\bar{\delta} = -0.04$ and $\sigma = 0.04$, values similar to those for component 2 of the wild-type protein (Figure 3B). This simulation also used an intrinsic EPR line width of $W = 18$ G, a value close to that used for wild-type protein.

Saturation–Recovery Studies of Wild-Type Compound ES

We have used the saturation–recovery method to reexamine the electron spin relaxation rates ($1/T_1$) of compound ES. In an earlier study we used CW methods to measure $1/T_1$ over the temperature range $1.9\ \text{K} \lesssim T \lesssim 4.2$ K. We found that relaxation of the radical of compound ES arises from an Orbach process (Abragam & Bleaney, 1970), which is exponential in temperature, as well as a simple phonon scattering process, which is linear in T:

$$\frac{1}{T_1} = aT + be^{-\Delta/T} \quad (9)$$

The Orbach process, which arises by thermally induced transitions to the excited spin states (see Figure 5), allows the zero-field splitting ($\Delta \simeq D_z$) and exchange coupling ($b \propto J^2 \propto \delta^2$) to be estimated (Hoffman et al., 1981). At ~3 K and above, the exponential term in eq 9 dominates; in contrast, at $T \lesssim 2$ K, the linear term dominates.

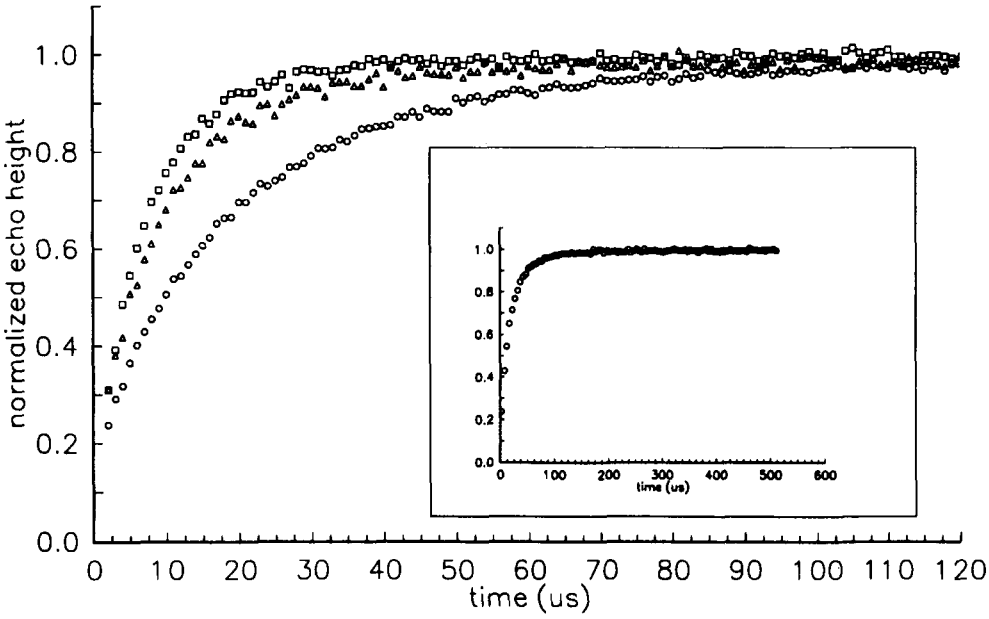

FIGURE 8: Saturation–recovery of wild-type compound ES at 4.2 K. The main figure shows the recovery of the signal from Trp-191 taken at three g values. The inset shows long-time data for $g = 2.011$. Experimental conditions: microwave frequency 9.4745 GHz; saturation sequence, described under Materials and Methods; detection sequence: $\pi/2$ (64 ns), $\tau = 296$ ns, π (128 ns); increment in delay time, T, of 1 μs per point; repetition rate, 10 Hz. The fields are 3365 G ($g = 2.011$) (△), 3395 G ($g = 1.994$) (○), and 3335 G ($g = 2.030$) (□).

In a saturation–recovery experiment the electron spin system is first saturated, and the return to thermal equilibrium is then measured. In the present work, the return is monitored as the height of a two-pulse electron spin echo. Figure 8 shows recovery traces at 4.2 K for compound ES taken at $g \approx 2.035$ on the low-field portion of the spectrum, at $g \approx 2.0$ near the EPR maximum, and at $g \approx 1.980$, on the high-field side. The data are approximately described by an exponential with $1/T_1$ ranging from $1/T_1 \approx 4 \times 10^4$ s^{-1} at $g \approx 2$ to 12×10^4 at $g \approx 2.04$. Upon cooling to $T \approx 2$ K the relaxation rate sharply decreases to $1/T_1 \approx 3 \times 10^2$ s^{-1} (not shown).

These results are consistent with the earlier CW measurements of Hoffman et al. (1981), including the field and temperature variation of $1/T_1$. They are equally consistent with the present model in that they show that $1/T_1$ is larger at $g \approx 2.04$ than at $g \approx 2.0$, as expected if $\Delta g \propto \delta$. However, the earlier analysis of spin relaxation rates indicated that the magnitude of J was much smaller than that required to explain the g shifts through use of eq 3. We now find that this conclusion was the result of an arithmetic error and that J as determined from the relaxation data is comparable in magnitude to that required by the distribution model. Both HRP and compound ES relax by an Orbach mechanism (Schulz et al., 1979), with $\Delta \approx D_z \approx 20$ cm^{-1} for HRP and $\Delta \approx 22$ cm^{-1} for compound ES. At 4.2 K the linear term in eq 9 can be ignored in both, and thus the ratio of J^2 for the two proteins can be estimated from the ratio of their relaxation rates. At 4.2 K and $g \approx 2.0$ the relaxation rate for HRP is $1/T_1 \approx 3 \times 10^6$ s^{-1} (Schulz et al., 1979), and the saturation–recovery value of $1/T_1$ for compound ES is given above. Taking $J \approx 1.4$ cm^{-1} for HRP (Schulz et al., 1979) and applying eq 9 to this rate ratio yields $J \approx 0.2$ cm^{-1} for compound ES. Given the uncertainty in the CW measurement of $1/T_1$ for HRP, and the lack of any attempt to account for a distribution in J, this is in more than adequate agreement with $\bar{J}_1 \approx 0.1$ cm^{-1} as calculated above.

The saturation–recovery measurements of electron spin relaxation have further been used to address the possibility that wild-type compound ES also exhibits a narrow, minority (~10%) free radical signal that displays resolved hyperfine couplings, most noticeably at $T \approx 77$ K (Hori & Yonetani, 1985; Goodin et al., 1987; Scholes et al., 1989; Fishel et al., 1991). In many years of studying wild-type compound ES (Hoffman et al., 1979, 1981), we have never observed such a signal either at $T \approx 77$ K or at $T \leq 4.2$ K. However, our efforts have emphasized the lower temperatures, $T < 4.2$ K. If such a radical exists and is remote from the heme, then at these temperatures its EPR signal would have an extremely long relaxation time and might be so easily saturated as to escape detection. Saturation–recovery measurements do not suffer from this uncertainty. They are capable of simultaneously detecting and characterizing overlapping signals from paramagnetic centers with widely different relaxation rates and should permit us to detect any species that relaxes on a time scale much slower than the majority species. Thus, we performed such measurements on wild-type compound ES, collecting data over long times at fields where only the majority spin-coupled signal can contribute, for example at $g \approx 2.04$, as well as at fields near $g \approx 2$, where the signal from an isolated radical would appear.

As seen in Figure 8, all the saturation–recovery traces reach the equilibrium magnetization within $T < 100$ μs, the recovery time for the Trp-191 radical. This figure shows no hint of another component that recovers more slowly within the time of this trace (500 μs). Similar experiments (data not shown) were performed on times of up to 4 s with the same, negative results. Thus, the saturation–recovery traces for wild-type compound ES at 4 K show there to be *no* significant amount of a second species near $g = 2.0$ that has markedly slower relaxation than the broad Trp-191 signal. As the dominant relaxation mechanism at 4 K for this latter signal is interaction with the $S = 1$ heme center, these observations imply that in this sample there is no significant signal associated with a radical center that is *remote* from the heme pocket. In contrast, the Trp-191 → Phe mutant exhibits a narrow signal from what is believed to be a Tyr radical. It has very slow spin–lattice relaxation and thus is believed to be remote from the heme (Gerfen et al., 1992). Clearly, our results indicate that the radical seen in this mutant is not present in native compound ES.

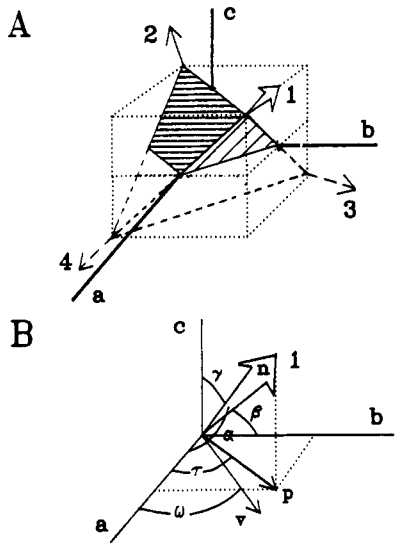

FIGURE 9: (A) Orientations of the heme normals in single crystal compound ES (Arrows). (B) Projection of the normal into the **ab** plane for single-crystal rotation in the **ab** plane.

Single-Crystal EPR

The conventional interpretation of the frozen-solution EPR spectrum of compound ES has been supported by the analysis of single crystal EPR measurements by Hori and Yonetani on high-spin ($S = {}^5/_2$) Fe^{3+}C*c*P and on compound ES (Hori & Yonetani, 1985). We now show that the distribution model not only gives a satisfactory interpretation of the frozen-solution EPR spectrum but also can account for the single-crystal measurements. We begin by describing the relevant crystal properties of C*c*P. We then summarize the findings of Hori and Yonetani and finally present the alternate interpretation.

X-ray crystallography has shown that crystals of C*c*P are orthorhombic with space group $P2_12_12_1$ and possess four molecules per unit cell (Finzel et al., 1984). These four molecules are related by 2_1 screw axes. In considering EPR measurements, the translational component of a screw axis can be ignored, and the **g** tensor of one reference molecule (site 1) can be used to generate the **g** tensors of the other three (sites 2–4) within a unit cell by 2-fold rotations about **a**, **b**, and **c**. In the crystal form observed for bakers yeast C*c*P, the heme normal, **n**, for the site we label "1" makes almost equal angles with respect to the crystal axes: $\alpha^n = 52°$, $\beta^n = 52°$, $\gamma^n = 60°$ (Finzel et al., 1984).[4] In this case, by the crystal symmetry, the four sites in a single crystal are then oriented so that the four heme normals approximately point to the four corners of a tetrahedron (Figure 9A); this would be precisely so for the case $\alpha^1 = \beta^1 = \gamma^1 = 54.7°$.

Because of the crystal habit, it was natural and reasonable for Hori and Yonetani to perform rotations of the crystal about the three principal axes **a**, **b**, and **c**, such that the field lies in a plane containing the other two crystal axes, **bc**, **ac**, and **ab**, respectively. In each such rotation the four molecules in a crystal of $P2_12_12_1$ space group are magnetically equivalent in pairs, so that the experimental spectra show only two signals. The results for Fe^{3+}C*c*P are depicted in Figure 10. The g^2 values of the two signals vary sinusoidally with the angle of rotation (ω) of the field in a coordinate plane relative to a

[4] The direction of the heme normal is taken to be the direction of the His-175 Fe bond as determined by the atomic positions reported by Edwards et al. (1987).

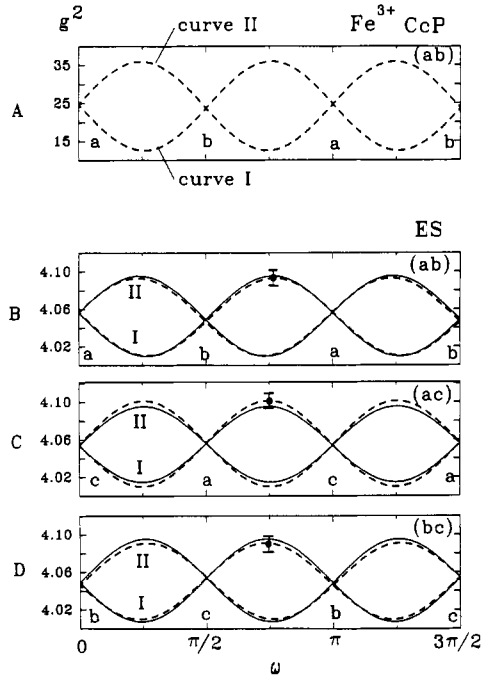

FIGURE 10: Single-crystal rotation study of Fe^{3+}C*c*P *and* compound ES. Dashed curves: angular variations of g^2 at 5 K taken from Hori and Yonetani (1985). (A) Fe^{3+} C*c*P in the **ab** plane. (B) Compound ES in the **ab** plane. (C) Compound ES in the **ac** plane. (D) Compound ES in the **bc** plane. Solid curves: Best fit to Hori and Yonetani's curves with eq B4 based on assignment of site 1 to curve I ($g_\perp = 2.024$, $g_\parallel = 1.992$ and $\alpha^{ES} = 56.2°$, $\beta^{ES} = 52.8°$, $\gamma^{ES} = 55.2°$). Error bars represent our estimate of error on g^2 in Hori and Yonetani's simulations, ±0.01.

particular coordinate axis and have extremal values at $\pi/4$, $3\pi/4$, etc., as depicted in Figure 10 for rotation in the **ab** plane. As seen in the figure, the ω dependencies of the two signals, as represented by curves I and II, are out of phase by approximately 90°; curve I has a minimum at $\pi/4$ and curve II has a maximum at $\pi/4$. The analysis by Hori and Yonetani of their experimental data gives $g_\parallel^{CcP} = 2.0$ lying along the heme normal and $g_\perp^{CcP} = 6 (g_\perp > g_\parallel)$ as expected from frozen-solution data, provided that curve I of Figure 10 is taken to correspond to site 1. The experimentally determined direction cosines of $g_\parallel$ with respect to the crystal axes correspond to angles of $\alpha^{HS} = 53°$, $\beta^{HS} = 51°$, and $\gamma^{HS} = 59°$ (Hori & Yonetani, 1985), in good agreement with (α^n, β^n, γ^n) given above.

An equivalent set of three rotations was performed with compound ES. Again two EPR signals that correspond to the broad Trp-191 signal characteristic of frozen solutions were seen for all orientations of the field in a coordinate plane. The angular dependencies are qualitatively similar to those of Fe^{3+}C*c*P with comparable sinusoidal dependencies on ω in all coordinate planes and with extrema at $\pi/4$, $3\pi/4$, etc., and a phase difference of ca. 90° (Figure 10). Likewise, they could be described by an axial **g** tensor. However, to achieve a result consistent with the conventional interpretation of the frozen-solution data, with $g_\parallel > g_\perp$ (and with all the attendant anomalies listed above), requires the assignment of curve II to site 1. This assignment leads to the reported values, $g_\parallel = 2.034$ and $g_\perp \approx 2.00$ (Hori & Yonetani, 1985). The corresponding direction arccosines of $g_\parallel$ ($\alpha^{ES} = 53°$, $\beta^{ES} = 58°$, $\gamma^{ES} = 54°$) are in good agreement with those for the heme normal and $g_\parallel$ of the high-spin ferriheme state.

To proceed, we reconsider these assignments in somewhat greater depth. This begins with explicit description of the

results expected when the field is rotated within a coordinate plane of a C*c*P crystal in which the paramagnetic state of the protein has a **g** tensor of axial symmetry, with $g_\parallel$ lying along the heme normal. For concreteness, consider the case where the field lies in **ab** and makes an angle ω with a; an equivalent analysis holds for rotation of the magnetic field in either of the other two coordinate planes, **bc** and **ac**. Site 1, whose normal lies in the (+**a**,+**b**,+**c**) octant is magnetically equivalent to site 2, whose normal lies in the (–**a**,–**b**,+**c**) octant, and this pair is distinct from sites 3 (–**a**,+**b**,+**c**) and 4 (+**a**,–**b**,–**c**), which form a second equivalent pair (Figure 9A). Therefore, it is sufficient to discuss just one site of each pair, sites 1 and 3. As shown in Appendix B, if we consider for clarity a slightly idealized crystal geometry, with the heme normals pointing exactly toward the corners of a tetrahedron, then the g values for sites i = 1,3 are related to the rotation angle of the field, ω, (Figure 9B) through the equation

$$g_{1,3}^2(\omega) = g_\perp^2 + (2/3)^{1/2}(g_\parallel^2 - g_\perp^2)\cos^2(\omega \pm \pi/4) \quad \text{(B2b)}$$

In agreement with the experimental data for Fe^{3+}C*c*P *and* compound ES, this equation has extrema at $|\omega| = \pi/4, 3\pi/4$, etc. The extremal values are

$$g^2(\pi/4; \text{site 1}) = g^2(3\pi/4; \text{site 3}) = (2/3)^{1/2}g^2 - [1 - (2/3)^{1/2}]g_\perp^2$$

$$= 0.816g_\parallel^2 - 0.184g_\perp^2$$

$$g^2(3\pi/4; \text{site 3}) = g^2(\pi/4; \text{site 1}) = g_\perp^2$$

The two magnetically inequivalent sites produce two curves out of phase by 90°. If $g_\perp < g_\parallel$, then the curve with a maximum at $\pi/4$, denoted curve II, is associated with site 1, and the curve with a minimum at $\pi/4$, denoted curve I, is from site 3. On the other hand, if $g_\perp > g_\parallel$, then curve II is from site 2, and curve I is from site 1. If we relax the restriction to the idealized geometry, then the more general eq B4 in Appendix B is applicable. However, the slight actual deviation of the heme normal from the idealized direction, $\alpha^1 = \beta^1 = \gamma^1 = 54.7°$, produces only minimal deviations from the idealized expression eq B2b; in particular, it does not change the correspondence between an assignment of a data curve to a crystal site and the relative magnitudes of $g_\parallel$ and $g_\perp$.

As noted above, Hori and Yonetani assigned site 1 to curve 1 for high-spin Fe^{3+}C*c*P. Their analysis of the data, which for an axial **g** tensor is equivalent to fitting the data to eq B4, gave the correct answer, $g_\perp \approx 6 > g_\parallel \approx 2$ with $g_\parallel$ roughly along the heme normal. According to eq B4 (or B2b), the alternate assignment, to curve II, would give the wholly unreasonable values of $g_\parallel^{CcP} \approx 3.8$ and $g_\perp^{CcP} \approx 7.1$ and thus is obviously to be discarded. In contrast, Hori and Yonetani assigned site 1 to curve II for compound ES. Their subsequent analysis of the single-crystal data, which again is equivalent to a fit with eq B4, gave results consistent with the conventional interpretation of frozen solution spectra, with $g_\parallel \approx 2.034$ and $g_\perp \approx 2.00$, and with $g_\parallel$ lying within ±5° of the heme normal. However, for compound ES, the alternate assignment of site 1 to curve I can describe the data equally well. As described in Appendix C, we used this assignment and fitted eq B4 to the g^2 rotation curves of Hori and Yonetani for all three coordinate planes. This fit gave optimal g values of $g_\perp = 2.024 > g_\parallel = 1.992$; the direction of $g_\parallel$ (direction arccosines, $\alpha^{ES} = 56.2°$, $\beta^{ES} = 52.8°$, $\gamma^{ES} = 55.2°$) corresponds well to the heme normal. Figure 10 compares the curves of Hori and Yonetani's rotation study with those from the fits based on the alternate assignment. Clearly, the alternative reproduces Hori and Yonetani's description of these data for rotations in the **ab**, **bc**, and **ac** planes to within the experimental error of the measured g values.

This refitting with $g_\perp > g_\parallel$ is in contradiction to the conventional interpretation of the frozen solution data, but it does correspond to expectations from eq 2 for spin coupling, and the g values themselves are quite reasonable with either assignment, unlike the case of the high-spin Fe^{3+}. In short, there is nothing in the reported single-crystal EPR study *itself* that distinguishes between the two assignments.

The resolution of this dilemma is provided in Appendix C, which considers the orientation dependence to be expected if the spin-coupled paramagnetic site of compound ES in a crystal is characterized by a distribution in δ. It is shown there that for a single-component distribution, $p_2(\delta)$, this model predicts that each site gives one line whose center can be described by an axial **g** tensor where $g_\parallel \approx 2.0$ should lie roughly along the heme normal and $\bar{g}_\perp = 2 + \bar{\delta}$ where $\bar{\delta}$ is the most probable g-shift parameter. For single-crystal rotations in a coordinate plane, there should be two lines that vary with the rotation angle ω in accordance with eq B4. But this is precisely the equation used with the alternate assignment. Thus, the alternate analysis of the single-crystal data is precisely consistent with the model developed above for the solution data and therefore is to be preferred over the conventional interpretation.

The value $g_\perp \approx 2.03$ obtained from the alternative fit to eq B4 corresponds to $\bar{\delta} \approx 0.03$ (eq 3). This most probable g-shift parameter is similar but not identical to that for component 1 in the simulation of the powder pattern. (It may be noted that Hori and Yonetani themselves calculated different $g_\parallel$ and $g_\perp$ in the analysis of their single-crystal data than for the powder EPR spectrum.) It is entirely plausible to assign the differences between frozen-solution and single-crystal data to slight differences in the most probable conformation about Trp-191 for a molecule in the two environments. The apparent absence of the second distribution component that is needed to simulate the frozen-solution spectrum of compound ES might mean that it is suppressed in the crystal, much as one component is suppressed in the spectrum of the D235E mutant. However, the second distribution is broader and more nearly isotropic than is the first distribution; a first-derivative spectrum would tend to obscure its position and even its presence. To test this possibility, we performed EPR and ENDOR measurements on a polycrystalline sample (data not shown). The EPR and ENDOR spectra are essentially the same as those from frozen-solution spectra, indicating that crystals of compound ES also exhibit two distributions in exchange coupling.

In principle, the alternate assignment of the curves for the single-crystal signals (Figure 10) could be distinguished experimentally from that of Hori and Yonetani with a measurement in which the field does not lie in any coordinate plane. However, the number of signals then increases from two to three or four because the magnetic equivalence within the pairs would be broken. Examination of the spectra obtained by Hori and Yonetani (1985) shows that it is unlikely that data of sufficient resolution could be obtained to distinguish between the two assignments unambiguously. Furthermore, the second, isotropic component seen in the single-crystal study would represent yet another signal and complicate the rotational dependence all the more.

DISCUSSION

This report has shown that wild-type compound ES and the ES(D235E) mutant have strikingly different 35-GHz EPR spectra, yet ^{1}H ENDOR measurements show that the radical site associated with the signal in both cases is a tryptophan, presumably Trp-191. These data, along with earlier observations summarized above, leave no doubt that the EPR signals under study cannot reflect a well-defined **g** tensor of an isolated radical. In particular, they conflict with the conventional interpretation, for which no molecular-level explanation has been offered, of EPR spectra of compound ES in terms of an axial **g** tensor with $g_\parallel \approx 2.04$ and $g_\perp \approx 2$.

Instead, the EPR signals have been explained in terms of a weak exchange coupling between the $S = 1$ oxyferryl heme and the radical on Trp-191, but with a distribution in the exchange-coupling parameter, J. A quantitative implementation of this model has been used to stimulate the frozen-solution spectra of the wild-type, ES(H,H), and the mutant, ES(D235E), proteins through the use of eq 8b. The theory presented here can describe the single-crystal EPR data of Hori and Yonetani through eq B4 just as well as the conventional picture. In addition, the present theory is wholly consistent with the *full* set of properties of the frozen-solution data, including the spin–lattice relaxation rates, and it is firmly based in the theoretical framework first developed by Debrunner and his co-workers (Schulz et al., 1979).

The theory has been presented at the formal level in terms of the spin Hamiltonian (eq 1) and the distribution in the g-shift parameter, $\delta = 2g_\perp^{Fe}(J/D)$ (eq 7). Mössbauer measurements can be analyzed in terms of a well-defined zero-field splitting parameter for the $(Fe{=}O)^{2+}$ center, $D_z \approx 22$ cm^{-1} (Schulz et al., 1979). This is the basis of the conclusion that the distribution in δ arises from a distribution in J, which in turn must reflect a distribution in protein conformations. A body of literature has grown around the investigation of protein conformational variability (Frauenfelder et al., 1991; Nocek et al., 1991), and it is now well accepted that a protein does not have one unique structure, but rather displays a range of "microstates". These interconvert rapidly in fluid solution but are frozen out at lower temperatures, often by $T \approx 200$ K. Thus, within limits, one may view the distribution detected in a low-temperature measurement as providing a "snapshot" of the relative populations of available protein conformations at the temperature where interconversion ceases.

The analysis of the compound ES EPR spectrum shows that the microstate distribution of the frozen-solution EPR spectra of compound ES is bimodal. The majority ($f_2 \approx 0.67$) of the molecules are described by a most probable g-shift parameter of $\bar{\delta}_2 \approx -0.01$, which corresponds to antiferromagnetic coupling of $\bar{J}_2 \approx -0.049$ cm^{-1}, and by a relatively broad distribution width of $\sigma_2 \approx 0.04$. The remainder of the molecules ($f_1 \approx 0.33$) have a most probable (ferromagnetic) coupling of $\bar{\delta}_1 = 0.02$, corresponding to $\bar{J}_1 \approx 0.098$ cm^{-1}, and a narrower distribution, $\sigma_1 \approx 0.02$ cm^{-1}. The Asp-235 → Glu mutation appears to abolish the form 1 microstates in frozen solution and to cause the entire population to fall within a distribution like that of form 2, with $\bar{\delta} = -0.04$ ($\bar{J} = -0.20$ cm^{-1}) and $\sigma = 0.04$. Given the tiny energies associated with the heme–radical spin coupling, it is hardly surprising that the EPR spectrum of compound ES should be exquisitely sensitive to small perturbations in the protein's surroundings (crystal vs solution) and to the subtle changes in structure that are seen to arise from the replacement of Asp by Glu at position 235 (Goodin & McRee, 1992). The X-ray studies show that Trp-191 touches the heme and is nestled against the proximal His with hydrogen-bonding by Asp (or Glu)-235 providing a bridge between N(δ) of His and the N–H of the Trp indole ring (Finzel et al., 1984). The results presented here certainly are consistent with a speculation that the weak spin coupling arises because the bridging hydrogen bond mediates an interaction between spin density of $(Fe{=}O)^{2+}$ that is delocalized onto the His (Thanabal et al., 1988) and spin density on the indole ring.

The single-crystal measurements likewise are well described by this theory provided that only a single population is invoked, with $\bar{\delta} \approx 0.03$ ($\bar{J} = +0.015$ cm^{-1}) and $g_\parallel = 1.994$. However, the measurements on a polycrystalline sample, which disclose a signal from the second component, make it likely that the difference between solution and crystal for the wild-type protein is more apparent than real, and that the signal from component 2 is missed in the crystal work because σ_2 is comparatively large. Its single-crystal EPR signal would be broad, and a first derivative spectrum would tend to obscure its presence.

These results for compound ES can be compared to those for compound I of HRP, where the radical resides on the porphyrin ring. In the latter case the EPR data can be interpreted[3] as arising from a distribution in J that is described by a sum of three component density functions, namely, $n = 3$ (eq 7) with $\bar{J}_1 = -1.3$, $\bar{J}_2 = 0.7$, and $\bar{J}_3 = 0.7$ cm^{-1}. That the exchange couplings in HRP are larger than those in compound ES can be attributed to the fact that the radical in HRP resides on the heme ring itself. In contrast, catalase[5] and chloroperoxidase (CPO) (Rutter et al., 1984) both *appear* to exhibit well-defined exchange coupling. However, in both of these enzymes $|\delta|$ is comparatively large, with the heme–radical coupling being antiferromagnetic in CPO and ferromagnetic in catalase. For these two proteins the apparent absence of a distribution in J arises because the same absolute spread in δ seen in HRP and compound ES represents a much smaller relative change in δ.

Fishel et al. have performed studies on other mutated forms of compound ES to find how perturbations near the Trp-191 radical site affect the EPR signal of the radical. It was found that the low-field, "$g \approx 2.04$", shoulder of the Trp-191 signal of wild-type compound ES shifts toward lower g value and the signal tends to sharpen with these mutations. We list their mutations near (but not at) Trp-191 in order of increasing perturbation (greater narrowing) of the EPR signal (Fishel et al., 1991):

Trp-223 → Phe
Met-231 → Leu
Met-230 → Ile
Met-230 → Tyr
Met-230, -231 → Leu, Leu
Asp-235 → Asn

The Asp-235 → Asn mutation left only a narrow radical-like signal similar to that of the Trp-191 → Phe mutant of compound ES mentioned above.

The researchers attribute this narrowing of the EPR signal to a decreasing *concentration* of the majority Trp-191 signal and a relative increase in concentration of a narrow, isotropic minority signal at $g = 2.004$. However, if this were so, then a relative increase in the intensity of the "narrow" signal would

[5] M. J. Benecky, J. E. Frew, N. Scowen, P. Jones, and B. M. Hoffman (to be published).

correlate with a decrease in the *intensity* of the broad signal, not with a narrowing of this signal. Our experiments with the compound ES mutant, Asp-235 → Glu, instead indicate that the distribution model must be considered in interpreting the results from these other mutants. Although the Asp-235 → Glu mutation results in a sharply altered EPR line shape, the ENDOR measurements show that this can in no way be interpreted as a relative increase in a hypothetical narrow signal at $g = 2.004$ or in a shift in the site of the radical. It is likely that many of the other mutations near Trp-191 that *partially* narrow the compound ES spectrum also do so because they affect the position or orientation of the Trp-191 radical with respect to the heme, thereby changing the center ($\bar{\delta}$) and/or breadth (σ) of the distribution in the exchange interaction, J. To settle this issue for other mutants, it would only be necessary to perform ENDOR studies such as those described here.

The question of a second radical site also arises for the wild-type compoound ES. As noted above, we have *never* seen such signals in our own wild-type samples even at $T \approx 77$ K [e.g., Hoffman et al. (1981)]. However, others have found evidence for a narrow, minority (~10%) signal in EPR spectra of wild-type compound ES in addition to the Trp-191 signal (Hori & Yonetani, 1985). A similarity in shape between this narrow signal of wild-type C*c*P and that in the Trp-191 → Phe protein prompted Fishel et al. (1991) to suggest that these may be the same. Because the radical signal of the Trp-191 → Phe mutant must reside at a different amino acid, they further suggest that the same is true for the minority signal in wild-type compound ES. This second site is proposed to be a Tyr, and in support of this assignment Fishel et al. (1991) show that the hyperfine splitting of the narrow signal strongly resembles that of the Tyr radical in photosystem II. As noted above, Gerfen et al. (1992) have proposed that the narrow radical signal seen in the Trp-191 → Phe mutant at 100 K in 140-GHz EPR spectra is from a Tyr that must be remote from the heme because it relaxes quite slowly.

The saturation–recovery and EPR experiments reported here directly address the issue of a second radical site remote from the heme in wild-type compound ES. The saturation–recovery measurements at $T \leq 4.2$ K show no paramagnetic species that relaxes at a greatly slower rate than the Trp-191 site. For comparison, the observed relaxation rate *at 100 K* for the remote Tyr radical in the Trp-191 → Phe mutant is orders of magnitude slower than any relaxation rate seen in our laboratory *at 4 K*. We conclude that well-prepared wild-type compound ES exhibits *no* signal from a second, remote site.

It may be that the narrow signal seen by some authors (Hori & Yonetani, 1985; Goodin et al., 1987) for wild-type compound ES at 77 K arises in samples that have a somewhat enhanced contribution from overoxidation. Alternatively, it may be seen the subset of molecules in the distribution that have vanishingly small J. The apparent similarity between such signals from Trp-191 in wild-type compound ES and the putative Tyr radical in ES(W191F) could arise because X-band and 35 GHz EPR are unable to resolve differences in g values for two similar aromatic radicals; this can be tested at 140 GHz. Likewise, the observation of hyperfine splittings in the signals from compound ES near $g \approx 2$ both in a single-crystal EPR study (Hori & Yonetani, 1985) and in frozen solution (Scholes et al., 1989; Fishel et al., 1991) also is interpretable within the distribution model. Those radicals for which $J \rightarrow 0$ should give sharp signals and might well display resolved hyperfine splitting. However, the close proximity of $S \approx 1$ $(Fe{=}O)^{2+}$ and Trp radical assure that T_1 will nonetheless be shortened, as indicated by our saturation–recovery data. The definitive way to resolve this issue to use isotopically labeled proteins to test the origin of the observed hyperfine couplings.

CONCLUSION

This paper offers a comprehensive explanation for the anomalous EPR spectra seen in frozen-solution and single-crystal studies of wild-type compound ES. The CW and pulsed EPR and the ENDOR data all can be understood in terms of a distribution in exchange couplings between the $S = 1$ $(Fe^{IV}{=}O)^{2+}$ moiety and the Trp-191 radical. The major change in the EPR spectrum of the Asp-235 → Glu mutant is shown to result from a change in the distribution of couplings, not from a change of the radical site. Similar changes in the spectra of other mutants may well have the same origin. The wild-type compound ES studied here gives no evidence for a second, minority signal associated with a different radical site and an alternate explanation of such observations is noted.

ACKNOWLEDGMENT

We thank Clark Davoust for his expert technical assistance and Thomas A. Doan for his mathematical assistance, as well as Eric Stemp and Dr. Debasish Kuila for their help in protein preparation.

APPENDIX A

The intensity of the EPR absorption envelope of a frozen-solution sample of compound ES in the limit where the individual molecules have a component line width of zero, I_p', represents the sum of signals at field, B, from all molecules for which the independent, random variables (θ,δ) give the appropriate g value through eqs 4 and 5. Thus, the intensity $I_p'(B)$ is the marginal probability density that a molecule resonates at field, B, taking all θ into account (Peterson & Kurkjian, 1972). The development of this function begins with the joint probability, $p_{12}(\delta,\theta)\, d\delta\, d\theta$, that a molecule in the sample simultaneously has g-shift parameter, δ, and that the Fe=O bond makes a polar angle, θ, with the applied field. Because δ and θ are independent random variables, the joint probability is the product of the two probabilities defined in eqs 6 and 7:

$$p_{12}(\delta,\theta)\, d\delta\, d\theta = p_2(\delta)p_1(\theta)\, d\delta\, d\theta$$

$$= p_2(\delta)\sin(\theta)\, d\delta\, d\theta \qquad \text{(A1)}$$

Converting this joint probability to the desired marginal probability requires a change of variable in eq 8 from (δ,θ) to (B,θ). First, eq 4 is solved for δ as a function of the new independent variables:

$$\delta(g^2,\theta) = \frac{g^2 - g_\parallel^2}{2g\sin^2\theta} \qquad \theta \neq 0 \qquad \text{(A2)}$$

$$\delta(B,\theta) = \left[\left(\frac{B_\parallel}{B}\right)^2 - 1\right]\frac{g_\parallel}{2\sin^2\theta} \qquad \text{(A3)}$$

where B is defined by eq 5 and

$$B_\parallel = \frac{h\nu}{\beta g_\parallel} \qquad \text{(A4)}$$

One can then write the joint probability that a molecule is oriented with an angle, θ, and that it resonates at a field, B,

as follows (Raghunathan, 1987):

$$p_3(B,\theta)\mathrm{d}B\mathrm{d}\theta = p_{12}(\delta,\theta)\mathrm{d}B\mathrm{d}\theta|J| \tag{A5}$$

where J is the Jacobian of the transformation

$$J = \begin{vmatrix} \frac{\partial\theta}{\partial\theta} & \frac{\partial\theta}{\partial B} \\ \frac{\partial\delta}{\partial\theta} & \frac{\partial\delta}{\partial B} \end{vmatrix} = \frac{\partial\delta}{\partial B} = \frac{B^2}{B^3}\frac{g^2}{\sin^2\theta} \tag{A6}$$

($\partial\delta/\delta\theta = 0$ because δ and θ are independent.) Finally, $I_p'(B)$, the marginal probability density that a molecule resonates at the given field, B, is obtained by integrating the joint probability density function, $p_3(B,\theta)$, over all θ (Walpole & Meyers, 1985):

$$I_p'(B) = \lim_{t\to 0}\int_t^{\pi/2} p_3(B,\theta)\,\mathrm{d}\theta \tag{A7}$$

$$I_p'(B) = \lim_{t\to 0}\int_t^{\pi/2} p_2(\delta)\left|\frac{\partial\delta}{\partial\theta}\right|\sin\theta\,\mathrm{d}\theta \tag{A8}$$

For compactness, we henceforth denote integrals such as that above as having a lower limit of $t = 0$.

The analysis to this point is independent of the functional form of the probability density function, $p_2(\delta)$. We choose to describe $p_2(\delta)$ as a weighted sum of normal (Gaussian) probability density functions, where each is centered around a most probable value, $\bar{\delta}_i$, with variance, σ_i^2, and each contributes to the sum with a fraction, f_i, where $\sum_i f_i = 1$:

$$p_2(\delta) = \sum_{i=1}^{n}\frac{f_i}{\sigma_i\sqrt{2\pi}}\exp\left[\frac{-1}{2}\left(\frac{\delta-\bar{\delta}_i}{\sigma_i}\right)^2\right] \tag{7}$$

Applying this density function of eqs A1, A5, and A6 gives the following result for the joint probability, $p_3(B,\theta)$:

$$p_3(B,\theta)\,\mathrm{d}B\,\mathrm{d}\theta = \left(\frac{B_\parallel^2}{B^3}\frac{g_\parallel^2}{\sin\theta}\right)\sum_{i=1}^{n}\frac{f_i}{\sigma_i\sqrt{2\pi}} \exp\left[-\frac{1}{2}\left(\frac{\delta(\theta,B)-\bar{\delta}_i}{\sigma_i^2}\right)^2\right]\mathrm{d}B\,\mathrm{d}\theta \tag{A9}$$

Combining eqs. A9 and A7 yields:

$$I_p'(B) = \sum_{i=1}^{n}\frac{f_i}{\sigma_i\sqrt{2\pi}}\int_0^{\pi/2}\frac{B_\parallel^2}{B^3}\frac{g_\parallel^2}{\sin\theta} \exp\left[-\frac{1}{2}\left(\frac{\delta(\theta,B)-\bar{\delta}_i}{\sigma_i^2}\right)^2\right]\mathrm{d}\theta \tag{A10}$$

In eq A10 above, a singularity occurs for $\theta = 0$. Although we have already stipulated in eq A2 that $\theta \neq 0$, the integral above is still allowed over the given limits because the exponential term approaches 0 much faster than $\sin\theta$ does. The envelope function actually observed in an EPR spectrum, $I_p(B)$, is a convolution of $I_p'(B)$ over the single-molecule component line shape and is given in eq 8 under Results and Analysis.

APPENDIX B

Consider a crystal of CcP where each molecule has a paramagnetic center with an axial **g** tensor, with $g_\parallel$ along the heme normal, **n**, and where we may write $g_\perp = g_\parallel + \delta$ without specifying whether δ is well-defined or distributional. Equation 3 gives the dependence of $g^2(\delta,\theta)$ on the angle, θ, between the heme normal and the applied field. We wish to describe the single-crystal spectrum for a rotation of the magnetic field in any of the three coordinate planes, **ab**, **bc**, and **ac**. For concreteness, we consider the field to lie in **ab** and to make an angle, ω, with **a** (Figure 9B). Site 1, whose normal points into the octant defined by (+**a**,+**b**,+**c**) and site 2 (–**a**,–**b**,+**c**) are magnetically equivalent and distinct from sites 3 (–**a**,+**b**,–**c**) and 4 (+**a**,–+b,–**c**). We explicitly discuss one site of each pair, sites 1 and 3. We define the unit vectors along the heme normal (**n**) and along the field vector (**v**), which lies in the **ab** plane:

$$\mathbf{n} = [\cos(\alpha), \cos(\beta), \cos(\gamma)]$$

$$\mathbf{v} = [\cos(\omega), \sin(\omega), 0]$$

Then, for a given heme the angle, θ, between the field and the normal is given by

$$\cos(\theta) = \mathbf{n}\cdot\mathbf{v} = \cos(\alpha)\cos(\omega) + \cos(\beta)\sin(\omega) \tag{B1}$$

In the slightly idealized case with the heme normals pointing exactly toward the corners of a tetrahedron, then $\alpha = \beta = 54.7°$, and eq B1 becomes

$$\cos(\theta_1) = (2/3)^{1/2}\cos(\omega - \pi/4)$$

$$\cos(\theta_3) = (2/3)^{1/2}\cos(\omega + \pi/4)$$

Thus, for a center described by the axial **g** tensor of eq 3

$$g_{1,3}^2(\omega) = g_\perp^2 + (g_\parallel^2 - g_\perp^2)\cos^2(\theta_{1,3}) \tag{B2a}$$

$$= g_\perp^2 + (2/3)^{1/2}(g_\parallel^2 - g_\perp^2)\cos^2(\omega \pm \pi/4) \tag{B2b}$$

Two EPR signals should appear and their orientation dependence should be out of phase by 90°. As discussed in the text, this function has extrema associated with the phase angles $\tau_i = \pm\pi/4, \pm 3\pi/4$, etc. where $i = 1$ and 3 for the heme sites.

In the real crystal, the extremal g values for a rotation in a coordinate plane do not fall precisely at $\tau_i = \pi/4, 3\pi/4$, etc., but actually fall along (and normal to) the vector, **p**, that corresponds to the projection of the heme normal onto **ab**, and can be written

$$\mathbf{p} = [\cos(\alpha^n), \cos(\beta^n), 0]$$

The slight deviations of **n** from the idealized directions shift the extrema to the phase angles, τ_i, i = 1–3,

$$\tau_i = \tan^{-1}\left(\frac{\cos(\beta_i)}{\cos(\alpha_i)}\right)$$

which correspond to the angles between **p** and the coordinate axes in Figure 9 (e.g., τ_1 is the angle between **p** and **a**). To see this we use this definition to rewrite

$$\mathbf{n} = [\sin(\gamma^n)\cos(\tau), \sin(\gamma^n)\sin(\tau), \cos(\gamma^n)]$$

which leads to

$$\cos\theta_i = \mathbf{n}\cdot\mathbf{v} = [\cos^2(\alpha_i^n) + \cos^2(\beta_i^n)]^{1/2}\cos(\omega - \tau_i)$$

$$\equiv \cos[\theta_i(\omega,\tau_i)] \tag{B3}$$

Insertion of eq B3 into eq B2a gives the final result,

$$g_{1,3}^2(\omega) = g_\perp^2 + (g_\parallel^2 - g_\perp^2)\cos^2[\theta(\omega,\tau_i)] \tag{B4}$$

Note that the sinusoidal dependencies of $g_{1,3}^2(\omega)$ are not out of phase by precisely $\pi/2$, but rather by 2τ.

The analysis by Hori and Yonetani of their single-crystal data for compound ES is equivalent to fitting those data to eq B4 under the assumption that site 1 gives rise to curve II in Figure 10. We wished to fit the single-crystal measurements for compound ES to eq B4 under the assignment of site 1 to curve 1. Given that Hori and Yonetani are able to *represent* these data with their assignment and their published **g** tensor, we chose to fit eq B4 to the curves generated from the published **g** tensor. An examination of the published spectra [e.g., Figure 6 of Hori and Yonetani (1985)] shows that the experimental uncertainties in the actual data must be appreciable, and thus this procedure is more than adequate. We return below to the discussion of errors. We performed a least-squares fit to curves of g^2 vs ω for the three coordinate planes, **ab**, **bc**, and **ac**, and obtained optimized values given in the text for $g_\parallel$ and $g_\perp$ as well as the orientation of $g_\parallel$ (α^{ES}, β^{ES}, γ^{ES}). Our results reproduce the *representation* of the Hori and Yonetani data quite well (Figure 10), with the maximum deviation in $g(\omega)$ of $\sim$0.002.

In fact, the plots in Figure 10 greatly overestimate any true discrepancies because they omit the uncertainties in the experimental data. An actual experimental spectrum in general contains two broad and ill-defined overlapping Trp-191 signals, and these are further overlapped by the far more intense, isotropic signal with resolved hyperfine structure. To estimate the error involved in determining the experimental g values of the two Trp-191 signals, we note that the signal from one pair of magnetically equivalent sites should be identical to that of the other pair after the magnet is rotated $\sim$90° (actually 2τ) away from the first orientation. Thus, the EPR spectrum with **B** along the **b** axis should be identical to the spectrum with **B** along the **a** axis. We have compared these spectra for rotation in the **ab** plane [see Hori and Yonetani (1985)] and find that the g values at which the intensity crosses 0 for orientations along **a** and **b** differ by 0.005 (2.004 vs 2.009). Thus, a measure of error in g^2 is $\Delta g^2 = 0.02$. Error bars of $\pm$0.01 are drawn in Figure 10 for comparison. Clearly the curves from the distribution model fit the data representation of Hori and Yonetani within this conservative estimate of error, and it is likely that as fits to the data the two analyses are of comparable quality.

APPENDIX C

To apply the model of a spin-coupled system with a distribution of δ to the single-crystal data, we recall that through eq 4, the g value depends on θ, the angle of the field with respect to the $g_\parallel$ axis of a site, and on the random variable δ. In the single-crystal experiment, the angle between the field and the heme normal of a site, θ, is fixed by the orientation of the crystal in the magnetic field and is no longer a random variable as it was in the frozen solution. However, we still presume that the molecules of the crystal also exhibit a distribution in δ. Below, we separate θ from the random variables by a semicolon to indicate this fact. We wish to calculate the value of g^2 for the maximum of the EPR signal for a given crystal orientation. To do this, we need to derive the intensity of the EPR signal as a function of g^2 for a given crystal orientation, $I_C(g^2;\theta)$. This quantity is merely the probability density that a subset of molecules with orientation, θ, will resonate at a given g^2 value (or field). In eq 7 we have already selected a particular form of the probability density, $p_2(\delta)$, where $\delta = \delta(g^2;\theta)$. Only a change of variable from δ to g^2, similar to that in eq A5, is needed to transform $p_2(\delta)$ to $I_C(g^2;\theta)$ (Raghunathan, 1987):

$$I_C(g^2;\theta)\, dg^2 = p_1(\delta)|J|\, dg^2$$

$$J = \frac{\partial \delta}{\partial g^2} = \frac{1}{2g \sin^2\theta} \qquad \theta \neq 0 \tag{C1}$$

where the Jacobian of the transformation, J, is found by solving eq 4 for δ in terms of g^2 and θ and then taking the derivative with respect to g^2. We begin by considering $p_1(\delta)$ in eq C1 to be a single normal density functions. Equation C1 then becomes

$$I_C(g^2;\theta) = \frac{1}{2\sigma\sqrt{2\pi}\, g_\parallel \sin^2\theta} \exp\left[\frac{-1}{2\sigma^2}\left(\frac{g^2 - \bar{g}^2(\theta)}{2g \sin^2\theta}\right)^2\right] \tag{C2}$$

The quantity $\bar{g}^2(\theta)$ is the orientation-dependent g^2 value (eqs 3 and 4) associated with the most-probable g shift (eq 2) that specifies the center of the Gaussian distribution in δ (eq 7). Equation C2 corresponds to an EPR signal that is a Gaussian when the field is expressed in terms of g^2. Equation C2 is not valid for describing line shapes at $g \approx g_\parallel$ and $\theta \approx 0$ because a singularity arises. In this region, the intrinsic EPR line width of the resonant molecules dominates the single-crystal EPR spectrum, and the proper intensity function is eq C2 convoluted with a line-shape function.

According to eq C2, the single-crystal signal is centered about a value, $\bar{g}^2(\theta)$, that depends on the orientation of the crystal in the magnetic field. The signal thus is described by the equation for an axial **g** tensor where $g_\parallel \approx 2.0$, $\bar{g}_\perp = 2 + \bar{\delta}$, and $\bar{\delta}$ is the most probable g-shift parameter. For the case of rotations in the three coordinate planes, the angle θ is given as a function of the rotation angle, ω, by eq B3, so that the signal in fact changes with ω according to eq B4.

REFERENCES

Abragam, A., & Bleaney, B. (1970) *Electron Paramagnetic Resonance of Transition Ions*, 2nd ed., Clarendon Press, Oxford.

Altschul, A. M., Abrams, R., & Hogness, T. R. (1940) *J. Biol. Chem. 137*, 777–794.

Atherton, N. M. (1973) *Ellis Horwood Series in Physical Chemistry: Electron Spin Resonance. Theory and Applications*, Halsted Press, New York, London, Sydney, and Toronto.

Box, H. C. (1977) *Radiation Effects: ESR and ENDOR Analysis*, Academic Press, New York.

Coulson, A. F. W., Erman, J. E., & Yonetani, T. (1971) *J. Biol. Chem. 246*, 917–924.

Dawson, J. H. (1988) *Science 240*, 433–439.

Edwards, S. L., Xuong, N. H., Hamlin, R. C., & Kraut, J. (1987) *Biochemistry 26*, 1503–1511.

Fan, C., Doan, P. E., Davoust, C. E., & Hoffman, B. M. (1992) *J. Magn. Reson. 98*, 62–72.

Finzel, B. C., Poulos, T. L., & Kraut, J. (1984) *J. Biol. Chem. 259*, 13027–13036.

Fishel, L. A., Villafranca, J. E., Mauro, J. M., & Kraut, J. (1987) *Biochemistry 26*, 351–360.

Fishel, L. A., Farnum, M. F., Mauro, J. M., Miller, M. A., Kraut, J., Liu, Y., Tan, X., & Scholes, C. P. (1991) *Biochemistry 30*, 1986–1996.

Frauenfelder, H., Sligar, S. G., & Wolynes, P. G. (1991) *Science 254*, 1598–1603.

Gerfen, G. J., Un, S., Bellew, B. F., Becarra, L. B., Singel, D. J., & Griffin, R. G. (1992), Rocky Mountain EPR Conference, Denver, Colorado.

Goodin, D. B., & McRee, D. E. (1993) *Biochemistry* (in press).

Goodin, D. B., Mauk, A. G., & Smith, M. (1986) *Proc. Natl. Acad. Sci. U.S.A. 83*, 1295–1299.

Goodin, D. B., Mauk, A. G., & Smith, M. (1987) *J. Biol. Chem. 262*, 7719–7724.

Goodin, D. B., Davidson, M. G., Roe, J. A., Mauk, A. G., & Smith, M. (1991) *Biochemistry 30*, 4953–4962.

Gordy, W. (1980) *Techniques of Chemistry, XV: Theory and Applications of Electron Spin Resonance*, John Wiley & Sons, New York.

Guigliarelli, B., More, C., Bertrand, P., & Gayda, J. P. (1986) *J. Chem. Phys. 85*, 2774–2778.

Hoffman, B. M., Roberts, J. E., Brown, T. G., Kang, C. K., & Margoliash, E. (1979) *Proc. Natl. Acad. Sci. U.S.A. 76*, 6132–6136.

Hoffman, B. M., Roberts, J. E., Kang, C. K., & Margoliash, E. (1981) *J. Biol. Chem. 256*, 6556–6564.

Hori, H., & Yonetani, T. (1985) *J. Biol. Chem. 260*, 349–355.

Hyde, J. S. (1979) in *Time Domain Electron Spin Resonance* (Kevan, L., & Schwartz, R. N., Eds.) Chapter 1, pp 1–30, John Wiley & Sons, New York.

Lang, G., Spartalian, K., & Yonetani, T. (1976) *Biochim. Biophys. Acta 451*, 250–258.

Larsson, L. O., Hagman, L.-O., Kierkegaard, P., & Yonetani, T. (1970) *J. Biol. Chem. 245*, 902–903.

Lerch, K., Mims, W. B., & Peisach, J. (1981) *J. Biol. Chem. 256*, 10088–10091.

Mauro, J. M., Fishel, L. A., Hazzard, J. T., Meyer, T. E., Tollin, G., Cusanovich, M. A., & Kraut, J. (1988) *Biochemistry 27*, 6243–6526.

McRee, D. E. (1992) *J. Mol. Graphics 10*, 44–46.

Moan, J., & Kaalhus, O. (1974) *J. Chem. Phys. 61*, 3556–3566.

Nocek, J. M., Stemp, E. D. A., Finnegan, M. G., Koshy, T. I., Johnson, M. K., Margoliash, E., Mauk, A. G., Smith, M., & Hoffman, B. M. (1991) *J. Am. Chem. Soc. 113*, 6822–6831.

Oosterhuis, W. T., & Lang, G. (1973) *J. Chem. Phys. 58*, 4757–4765.

Peterson, G. E., & Kurkjian, C. R. (1972) *Solid State Commun. 11*, 1105–1107.

Raghunathan, P. (1987) in *Electronic Magnetic Resonance of the Solid State* (Weil, J. A., Bowman, M. K., Morton, J. R., & Preston, K. F., Eds.) Chapter 13, pp 175–186, The Canadian Society for Chemistry, Ottawa.

Roberts, J. E., Hoffman, B. M., Rutter, R., & Hager, L. P. (1981) *J. Biol. Chem. 256*, 2118–2121.

Rutter, R., Hager, L. P., Dhonau, H., Hendrich, M., Valentine, M., & Debrunner, P. (1984) *Biochemistry 23*, 6809–6816.

Scholes, C. P., Liu, Y., Fishel, L. A., Farnum, M. F., Mauro, J. M., & Kraut, J. (1989) *Isr. J. Chem. 29*, 85–92.

Schulz, C. E., Devaney, P. W., Winkler, H., Debrunner, P. G., Doan, N., Chiang, R., Rutter, R., & Hager, L. P. (1979) *FEBS Lett. 103*, 102–105.

Sivaraja, M., Goodin, D. B., Smith, M., & Hoffman, B. M. (1989) *Science 245*, 738–740.

Thanabal, V., La Mar, G. N., & de Ropp, J. S. (1988) *Biochemistry 27*, 5400–5407.

Walpole, R. E., & Meyers, R. H. (1985) *Probability and Statistics for Scientists and Engineers*, 3rd ed., MacMillan Publishing Co., New York.

Wittenberg, B. A., Kampa, L., Wittenberg, J. B., Blumberg, W. E., & Peisach, J. (1968) *J. Biol. Chem. 243*, 1863–1870.

Yonetani, T. (1965) *J. Biol. Chem. 240*, 4509–4514.

Yonetani, T. (1976) in *The Enzymes* (Boyer, P. D., Ed.) Vol. 13, Chapter 6, pp 345–361, Academic Press, Orlando, FL.

Yonetani, T., Schleyer, H., & Ehrenberg, A. (1966) *J. Am. Chem. Soc. 241*, 3240–3243.